Acta Mech Sin (2009) 25:471–479
DOI 10.1007/s10409-009-0248-4

RESEARCH PAPER

Studies of the unsteady supersonic base flows around three afterbodies

Zhixiang Xiao · Song Fu

Received: 16 June 2008 / Revised: 25 November 2008 / Accepted: 5 January 2009 / Published online: 24 March 2009

Abstract Unsteady supersonic base flows around three afterbodies, cylindrical (Cy), boattailed (BT) and three-step (MS), are investigated in this paper. Reynolds-averaged Navier–Stokes (RANS) and two RANS/LES (large-eddy simulation) hybrid methods, detached eddy simulation (DES) and delayed-DES (DDES), are used to predict the base flow characteristics around the baseline Cy afterbody. All the RANS and hybrid methods are based on the two-equation SST (shear-stress transport) model with compressible corrections (CC). According to the comparison of measurements, both DES and DDES can produce more satisfactory results than RANS. RANS can only present the "stable" flow patterns, while the hybrid methods can demonstrate unsteady flow structures. DDES and DES results are little different from one another although the latter exhibits better agreement with the experiment. DES is taken to investigate the 5° BT and three-step afterbodies. The mean flow data and the instantaneous turbulent coherent structures are compared against available measurements.

Keywords Cylindrical · Boattailed and three-step afterbodies · DES and DDES · Unsteady flow

The project supported by the National Natural Science Foundation of China (10502030 and 90505005), Innovation and Support Foundation of Chinese Astronautics.

Z. Xiao (✉) · S. Fu
School of Aerospace Engineering,
Tsinghua University, 100084 Beijing, China
e-mail: xiaotigerzhx@tsinghua.edu.cn

1 Introduction

Base flow is one of the fundamental fluid mechanics problems occurring in flows around bluff bodies, such as projectiles, missiles, rockets, spaceships, or ground vehicles like cars, trucks, trains, etc. The aerodynamic characteristic at the base strongly influences the drag and stabilities of these moving objects. The low pressure behind the base due to the recirculation commonly existing there can cause significant amounts of total drag (40% or more), especially for a missile in unpowered flight stage, where the high pressure and high momentum jet is unavailable. If the base drag is effectively reduced, the flight range or the payloads can be significantly extended.

As is known, increase in the base pressure leads to the drag reduction. The aim of the base drag reduction methods is thus to increase the base pressure. Base drag reduction concepts basically fall in two forms, active and passive methods. Active methods can reduce the base drag by introducing high pressure gas directly. Even thrust could be achieved. However they need additional devices and complex control system. The active methods include bleeding [1], burning, etc. Small modifications of the afterbody geometry can be considered as effectively passive drag reduction methods, which do not alter base structures design and induce little drag increase, such as BT [2], channel [3], MS [4], square [5], etc. The passive approach will be focused in this work.

Among the passive methods, the BT or conical concept is very popular and proved very effective in reducing base drag. However, to achieve more drag reduction, the length of conical afterbody has to be sufficiently long because a short BT afterbody does not offer necessary pressure recovery on the base surface. Application of shorter, lighter and lower cost afterbody with possibly less base drag is the perfect objective for designers. MS afterbody is another concept which can effectively reduce the base drag through controlling the

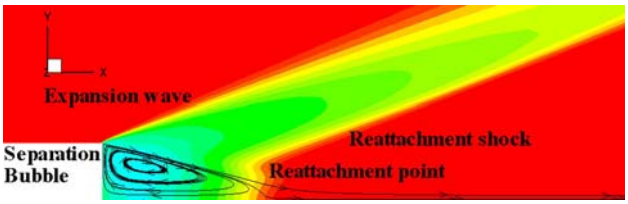

Fig. 1 The sketch of supersonic base flows with streamlines highlighting the base recirculation

separation before the base. It can offer less base drag, shorter afterbody length and lighter structure with careful optimization of the afterbody geometry. They can also achieve friction reduction due to the recirculation behind the sub-steps. Both BT and MS afterbodies are easy to implement in practice and to achieve the drag reduction effectively.

Although the geometry of the Cy baseline afterbody is very simple, the flow (as shown in Fig. 1) behind the base contains very complex flow phenomena, such as rapid expansion/reattachment shock waves, shock/vortex interaction, shear flow/recirculation interference, and high frequency unsteady wake, etc. The Cy afterbody had been extensively investigated with experimental [6,7], semi-empirical and numerical approaches.

In recent years, numerical approaches, such as solving RANS [8–10] with various turbulence models, large-eddy simulations (LES) [11], direct numerical simulations (DNS) [12] and RANS/LES hybrid methods [13–17], had been developed to explore the characteristics of base flow with the rapid development of computers resource and computational methods. Varying degrees of success had been achieved as all the prediction methods have their own advantages and limitations in this flow application.

Although there are many unanswered questions including the turbulence modelling uncertainty the RANS method with turbulence models are widely used for analyzing the afterbody design options. Also, the flowfields by solving RANS with turbulence models are often taken as the initial fields for the calculation with more advanced turbulence models such as the RANS/LES hybrid methods [13–16]. In fact, the RANS method with popular turbulence modelling could not often reliably provide satisfactory agreements with the experiments. The RANS methods had been developed to predict many of the important mean flow characteristics, such as the force, moment and velocity, etc., but it was not intended to simulate the complex unsteady coherent structures, pressure fluctuations or turbulent stresses.

LES is a powerful tool for resolving the large, energy-containing scales of unsteady motion that are typically time- and geometry-dependent. However, the sub-grid scale models for the boundary layer and compressible flows are not sufficiently well-developed to accurately predict the supersonic base flows. At the same time, LES require almost the same grid cells as direct numerical simulation (DNS) for high Reynolds number flows near the wall.

Limited by computational cost, the combination of LES with RANS can achieve both reasonably high efficiency and numerical accuracy for the base-flow applications. To make the best use of RANS and LES, an alternative modelling strategy of turbulent flows, often called as RANS/LES hybrid methods [13,17,18], has recently been proposed to predict the unsteady and geometry-dependent separating flows. Such hybrid methods combine a high-efficiency turbulence model near the wall, where the flow is dominated by small scale motion with an LES-type treatment for the large scale motion in the flow region far away from the wall. Therefore, the core idea of the hybrid methods is to combine RANS near the wall with LES in the separation region. The fundamental turbulence models still significantly affect the predicted flow characteristics for missile application. To construct the hybrid RANS/LES methods rationally, one generally hopes that the turbulence model has good numerical properties and has a *low-Reynolds-number* capability to resolve the near-wall turbulence characteristics.

The two-equation k–ω model, for its favourable numerical aspects, is commonly taken as an appropriate choice even though the original version proposed by Wilcox [19] although it often suffers from undesirable freestream-dependence. The SST model [20] is a hybrid approach through coupling the k–ω model in the near-wall region with the less freestream-dependent k–ε model outside the boundary layer. This model considers the transport of the principal turbulent shear stress and shows a good capability for modelling adverse pressure gradients flows. The original SST model did not include CC. In order to keep the desirable near wall behaviour of Menter's model and to improve the behaviour of shear layer, Suzen [9], however, added compressible dissipation and pressure dilatation terms only to the k–ε portion.

In the present work, the DES [16,21] and DDES [22–24] based on SST model with CC are used to investigate the different flow characteristics around different configurations, including the baseline, five-degree BT and three-step afterbodies (both BT and MS have the same base area). The detailed results of Cy afterbody are presented to validate the numerical and turbulence modelling methods.

2 SST model with CC and the RANS/LES hybrid methods

This zonal model uses Wilcox's k–ω model, which well behaves near solid walls and needs no low-Reynolds number corrections. At the same time, it combines with the standard k–ε model (reformulated in a k–ω style), which is relatively insensitive to free-stream values in the outer edge of the boundary layer and free stream. The switching is realized by

a flow dependent blending function F_1. The SST model also limits the eddy viscosity by forcing the turbulent shear stress to be bounded by constant times the turbulent kinetic energy inside boundary layers (a realizability constraint). This modification improves the model's performance on flows with strong adverse pressure gradients and separation. The mathematical forms of the turbulence equation including CC can be given as follows:

$$\frac{\partial \rho k}{\partial t} + \frac{\partial}{\partial x_j}\left[\rho u_j k - (\mu + \sigma_k \mu_t)\frac{\partial k}{\partial x_j}\right] = \tau_{ij} S_{ij} - \left[1 + \alpha_1 M_t^2 (1 - F_1)\right]\beta^* \rho k \omega + (1 - F_1)\overline{p'' d''}, \tag{1}$$

$$\frac{\partial \rho \omega}{\partial t} + \frac{\partial}{\partial x_j}\left[\rho u_j \omega - (\mu + \sigma_\omega \mu_t)\frac{\partial \omega}{\partial x_j}\right] = \gamma \frac{\omega}{k}\tau_{ij} - \beta \rho \omega^2 + 2(1 - F_1)\frac{\rho \sigma_{\omega 2}}{\omega}\frac{\partial k}{\partial x_j}\frac{\partial \omega}{\partial x_j} + (1 - F_1)\alpha_1 M_t^2 \beta^* \rho \omega^2 - (1 - F_1)\overline{p'' d''}/\nu_t, \tag{2}$$

where $\tau_{ij} = 2\mu_t(S_{ij} - S_{kk}\delta_{ij}/3) - 2\rho k \delta_{ij}/3$ is the Reynolds-stress tensor modelled by the Boussinesq eddy-viscosity hypothesis; S_{ij} is the strain rate defined as $(\partial u_i/\partial x_j + \partial u_j/\partial x_i)/2$; the constant $\beta^* = 0.09$; M_t is the turbulence Mach number which is defined as $\sqrt{2k}/a$ where a is the sonic; the pressure dilatation term is $\overline{p'' d''} = -\alpha_2 \tau_{ij} \partial u_i/\partial x_j M_t^2 + \alpha_3 \rho \beta^* k \omega M_t^2$; The closure coefficients for the compressible corrections are: $\alpha_1 = 1.0, \alpha_2 = 0.4, \alpha_3 = 0.2$. The blending function F_1 is defined as:

$$F_1 = \tanh\left\{\left[\min\left(\max\left(\frac{\sqrt{k}}{0.09\omega d}; \frac{500\mu}{\rho d^2 \omega}\right); \frac{4\rho \sigma_{\omega 2} k}{C D_{k\omega} d^2}\right)\right]^4\right\} \tag{3}$$

and the cross diffusion $C D_{k\omega} = \max\left(\frac{2\rho\sigma_{\omega 2}}{\omega}\frac{\partial k}{\partial x_j}\frac{\partial \omega}{\partial x_j}; 10^{-10}\right)$; d is the distance from the nearest wall. Some other constants are calculated from $\phi = F_1\phi_1 + (1 - F_1)\phi_2$, where the ϕ's are the constants: $\sigma_{k1} = 0.85$, $\sigma_{\omega 1} = 0.5$, $\beta_1 = 0.075$, $\gamma_1 = \beta_1/\beta^* - \sigma_{\omega 1}\kappa^2/\sqrt{\beta^*} = 0.553$; $\sigma_{k2} = 1.0$, $\sigma_{\omega 2} = 0.856$, $\beta_2 = 0.0828$, $\gamma_2 = \beta_2/\beta^* - \sigma_{\omega 2}\kappa^2/\sqrt{\beta^*} = 0.44$ and $\kappa = 0.41$.

The eddy-viscosity of SST model is defined as

$$\mu_{t,\mathrm{SST}} = \min\left(\frac{\rho k}{\omega}; \frac{\rho a_1 k}{\Omega F_2}\right), \tag{4}$$

where Ω is the magnitude of the vorticity defined as $\Omega = \sqrt{2 W_{ij} W_{ij}}$ with $W_{ij} = (\partial u_i/\partial x_j - \partial u_j/\partial x_i)/2$, denoting the rate of rotation tensor; $a_1 = 0.31$; and $F_2 = \tanh\left\{\left[\max\left(2\frac{\sqrt{k}}{0.09\omega d}; \frac{500\mu}{\rho d^2 \omega}\right)\right]^2\right\}$ is another blending function.

To construct a DES-type hybrid method based on two-equation k–ω models, transformation is adopted for the destruction term in the turbulent kinetic energy transport equation. After introducing a length scale, Eq. (1) can be rewritten as

$$\frac{\partial \rho k}{\partial t} + \frac{\partial}{\partial x_j}\left[\rho u_j k - (\mu + \sigma_k \mu_t)\frac{\partial k}{\partial x_j}\right] = \tau_{ij} S_{ij} - \left[1 + \alpha_1 M_t^2 (1 - F_1)\right]\beta^* \rho k \omega \cdot F_{\mathrm{DES}} + (1 - F_1)\overline{p'' d''}, \tag{5}$$

where F_{DES} is the hybrid function defined as

$$F_{\mathrm{DES}} = \max\left[(1 - F_{\mathrm{SST}}) \cdot \frac{L_t}{C_{\mathrm{DES}}\Delta}; 1\right] \tag{6}$$

and the turbulence length scale L_t is defined as $L_t = k^{1/2}/(\beta^* \omega)$; $C_{\mathrm{DES}} = F_1 \times 0.78 + (1 - F_1) \times 0.61$; Δ is the grid scale defined as $\Delta = \max(\Delta x, \Delta y, \Delta z)$; F_{SST} can be taken as 0, F_1 or F_2. If $F_{\mathrm{SST}} = 0$, the hybrid method reverts to a Strelets-type [18] DES method. If $F_{\mathrm{SST}} = F_1$ or F_2, then, this hybrid approach is called the delayed-DES method [23,24]. Due to the numerical properties of F_1 and F_2, $(1 - F_{\mathrm{SST}})$ approaches zero near the wall and the DDES will act in the RANS mode. At the same time, $(1 - F_{\mathrm{SST}})$ becomes zero out of the boundary layer and the DDES goes to the original Strelets-type DES model. Therefore, DDES can ensure itself to act in the RANS mode near the wall without the effects on the locally clustered grid scales. In other words, DDES can delay the switching from RANS to LES near the wall due to the grid scales, especially the locally refined grids in the streamwise and spanwise direction for the complex missile configurations. In this paper, F_{SST} is taken as F_2.

The ω-equation and the eddy viscosity definition are the same as that in the SST model with CC. In the Strelets-type DES method (i.e. $F_{\mathrm{SST}} = 0$), when $L_t/(C_{\mathrm{DES}}\Delta) < 1$, $F_{\mathrm{DES}} = 1$, the hybrid method acts in the RANS mode. When $L_t > C_{\mathrm{DES}}\Delta$, the method acts in the Smagorinsky LES mode. When turbulence production is balanced by the dissipation term, $P_k = \rho \nu_t \tilde{S}^2 = D_k = \rho k^{3/2}/L_t$, $k = \beta^* L_t^2 \tilde{S}^2$ and $L_t = C_{\mathrm{DES}}\Delta$. Then the eddy viscosity can be rewritten as

$$\nu_t = (\beta^*)^{3/2}(C_{\mathrm{DES}}\Delta)^2 \tilde{S} \propto \Delta^2 \tilde{S}. \tag{7}$$

From Eq. (7), the eddy viscosity is similar as that of Smagorinsky's model. When the grid is locally refined, the hybrid method will act as in an LES mode.

3 Numerical methods

The computations in this article are all based on a compressible solver using Roe flux-difference splitting scheme with 5th-order weighted essential non-oscillatory (WENO) and Radespiel–Swanson entropy fix in a cell-centered finite-volume formulation. A modified fully implicit LU-SGS with Newton-like sub-iteration in pseudo time is taken as the time marching method when solving the mean flow equations

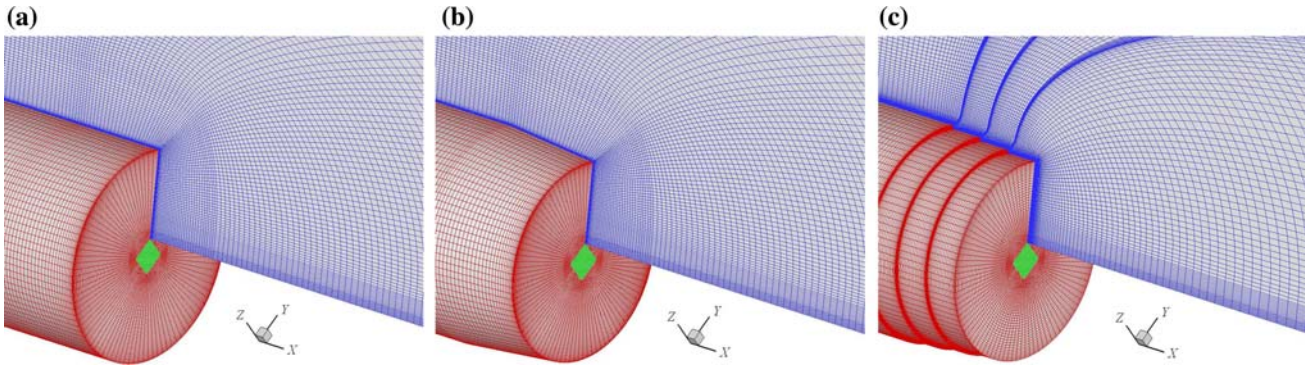

Fig. 2 The three base-configurations and grids (from *left* to *right*, Cy, BT and MS)

and the turbulence model equations. Global non-dimensional time stepping ($\Delta t = 0.005$) is implemented to capture the unsteady properties of the separation flows, where the physical time is corresponding to 1.37×10^{-6} s [6,7]. It also indicates that the RANS here is the unsteady-RANS case. Nevertheless, most of the results here are time-averaged unless specified. The approach is parallelized using domain-decomposition and message-passing-interface strategies for the platform on PC clusters with 64-bit AMD Athlon 3200+.

Because the effect on grid number around the baseline configuration was investigated before [16], similar grid density is adopted in this paper. Two-block grids ($111 \times 97 \times 161 + 25 \times 25 \times 161 \cong 1.83$ million cells for Cy and BT cases and $161 \times 97 \times 161 + 25 \times 25 \times 161 \cong 2.61$ million cells for MS case) are used to avoid the singularity of the base centre, as shown in Fig. 2. The base area of MS is the same as the BT one and the ratio of length over height are the same as each other. The ratio of length over height of each sub-step is arctan (5°) (i.e. $\eta = l/h = \arctan(5°) \cong 11.43$).

In this paper, $x/D = 0$ is set at the base surface. The inlet conditions are fixed and prescribed at $x/D = -1.0$ using the experimental measurements (streamwise velocity profiles) [6]. The outflow boundary is at $x/D = 15$ with zero streamwise gradients due to the supersonic freestream and the non-reflection boundary condition with 1-D Riemann invariant. The periodical condition is applied at the circumferential direction for the outer block. No-slip conditions are applied on the wall. For computational convenience, "Ghost cells" are used to treat all kinds of boundary conditions including the boundaries of the adjacent zonal domains and different PC clusters.

4 Results and discussion

4.1 Flow around the baseline configuration

Flow conditions of the supersonic axisymmetric base flow are based on the experiments [6,7]. In accordance with the experiments, the freestream Mach number is set to 2.46, and the Reynolds number based on the cylinder diameter ($D^* = 63.5$ mm) is 2.858×10^6, and the angle of attack is taken as 0°.

4.1.1 Comparisons on CC

As we know, the fundamental turbulence models have an important influence on the RANS/LES hybrid methods. Therefore, the effect on CC should be investigated first.

According to Fig. 3, the velocity components of the flow can clearly reflect the difference of SST model with and without CC. The u-velocity without CC at the central line shows deviation from that of CC and of the measurements, especially at the positions far from the base. The streamwise-velocity with CC matches the measurements well except the shear layer. Little difference about the radial velocity is demonstrated.

From the streamwise-velocity comparisons, it also indicates that the SST model with CC can predict the rear stagnation position of the recirculation well than that of SST model without CC.

4.1.2 Comparisons on RANS, DES and DDES

Figure 4 shows the comparisons of the streamwise and radial velocity components, streamwise normal stress $\langle uu \rangle$ component at several downstream positions after the base and base pressure coefficients between the experiments [6] and computation results obtained with RANS, DES and DDES, which are all based on the SST model with CC.

The magnitude of streamwise velocity from RANS is significantly larger than the measurements near the base centre which corresponds to an adverse pressure gradient larger than the experiment. Near the shear layer, the hybrid methods show better agreement with the measurements both in the streamwise and radial velocities. Although all the numerical results shows some departure from the measurements, especially near the base, the normal stress component $\langle uu \rangle$ by RANS is relatively much weaker than those from hybrid methods and DES gives slightly more satisfactory results

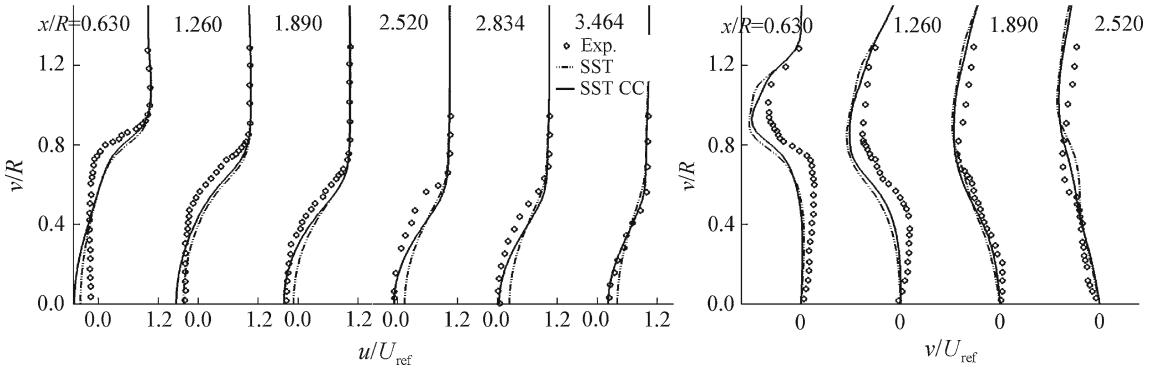

Fig. 3 Comparisons on the velocity components at several streamwise positions around Cy afterbody (RANS)

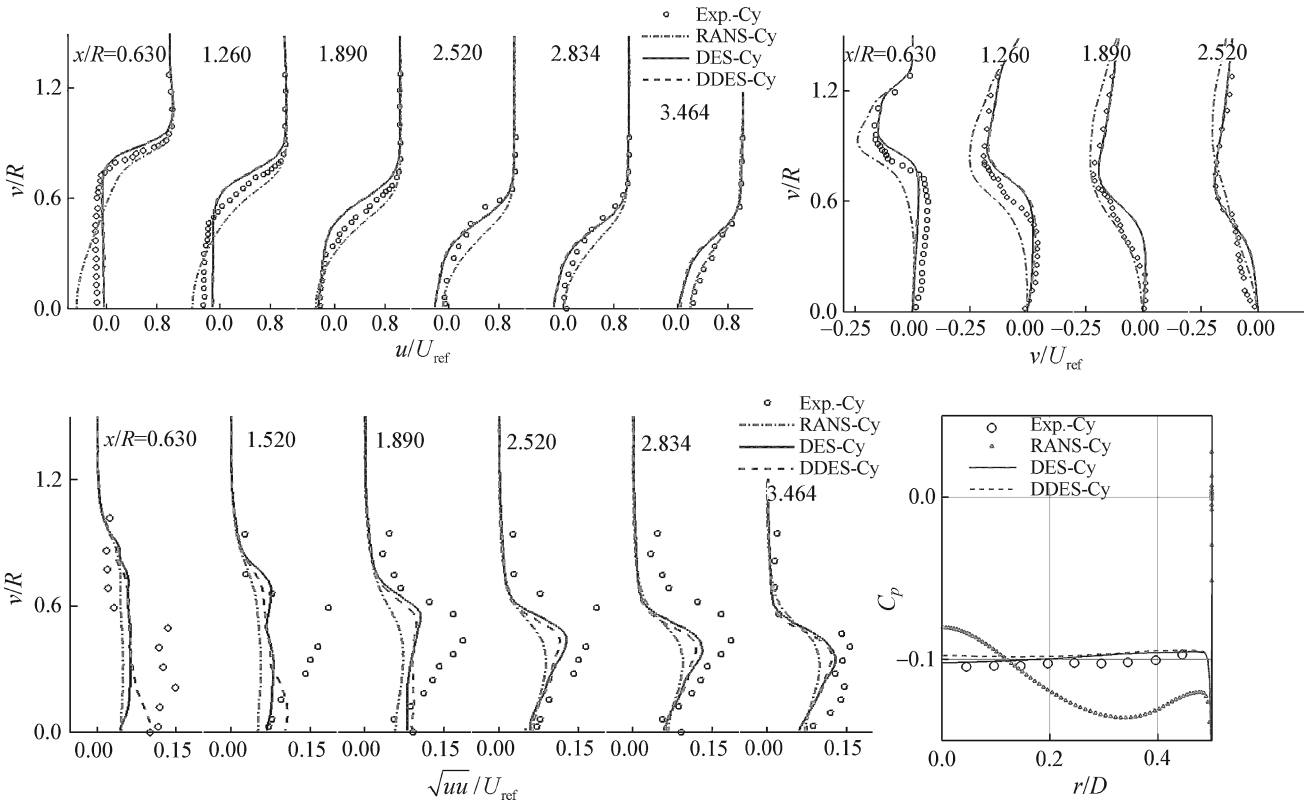

Fig. 4 Comparisons on velocity components, streamwise normal stress and pressure on the base

than those of DDES. The experiment shows that the pressure at the base is basically uniform. From Fig. 4, RANS does not accurately predict the pressure distribution well leaving large variation in the pressure distribution in the radial direction. The hybrid methods, especially the DES, can predict the pressure distribution on the base very well. Therefore, DES based on the SST with CC is taken as the baseline numerical prediction method for the flows around the BT and MS afterbodies.

Figure 5 presents Mach-number contours after the base using DES and RANS. DES shows evident unsteady small-scale structures behind the base and in the wake; RANS only predicts the stable and smooth primary recirculation.

Figure 6 presents the history of non-dimensional pressure at the position xyz (0, 0, 0.45) on the base wall. From this figure, the pressure "converges" very fast after 0.005 s in RANS calculation. Both DES and DDES demonstrate the unsteady and turbulent characteristics with a larger mean value than those of RANS. It can be deduced here that the pressure drag predicted by DES and DDES is less than that with RANS.

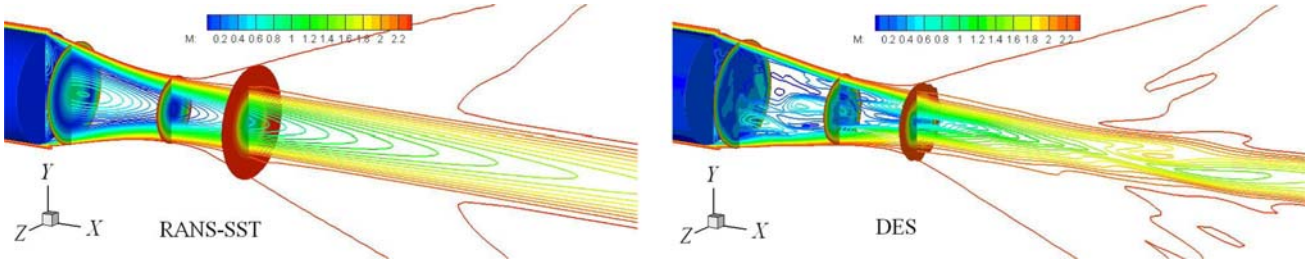

Fig. 5 The Mach number contours behind the base (instantaneous, Mach number range is from 0 to 2.4)

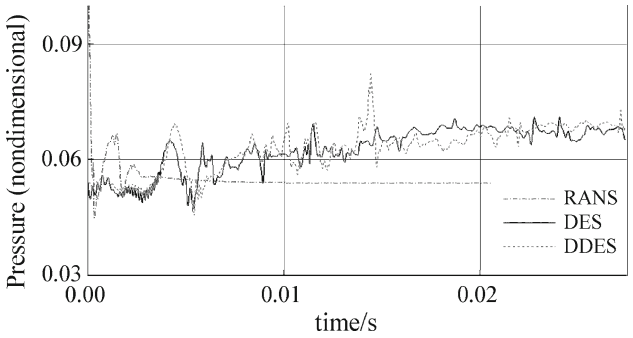

Fig. 6 The history of pressure on the base wall at xyz (0, 0, 0.45)

4.2 Comparisons on different afterbodies

Figure 7 presents the pressure coefficients on the wall of base and afterbody. The measurements on the base for Cy and BT afterbodies are available from Herrin and Dutton [2,6]. The numerical results are all obtained using the DES because it can presents more satisfactory results in the Cy case as shown in the comparisons and analysis before. At the base, the pressure coefficients between the BT and MS show little difference from each other, the MS afterbody has similar base pressure drag as that of BT. It is important to note that both BT and MS afterbodies give a reduction in the level of the pressure coefficient as shown in Fig. 7. Of course, BT afterbody can afford a little higher pressure recovery on the base, which means that more base drag reduction can be achieved.

In the streamwise direction, the surface pressure on the BT afterbody matches the measurements very well, and the pressure coefficients on the MS afterbody are very complex due to the sub-steps strting at $x/D = -0.5$ before the main base. After each sub-step, the pressure decreases rapidly indicating the existence of sub-base drag. However, the pressure encounters recovery along the sub-step, although it can not resume as the Cy case.

Figure 8 presents the streamwise and radical velocities at several streamwise positions around the three configurations. From the flow structures behind the base, the velocities around the BT and MS differ insignificantly from each other, the velocity of Cy afterbody shows more distinct departure from them. From this figure, the level of the normal stress $\langle uu \rangle$ of cylindrical case is generally higher than those of BT and MS, and the position of the maximum stress is more outward in the radial direction.

Figure 9 shows the instantaneous contours of $Q(= S_{ij}^2 - \Omega^2)$ around Cy, BT and MS configurations obtained from DES calculations. Helical coherent structures in the shear layer can be detected clearly. DES can capture streamwise structures present within the recirculation region and in the developing wake. It can be seen that the flow structures in all the three cases are all similar, i.e., the small change in geometry does not significantly alter the nature of the structures. Helical structures are visible behind the base. For the little steps, MS geometry is covered with the streamwise vortices before the primary base and the streamwise flow

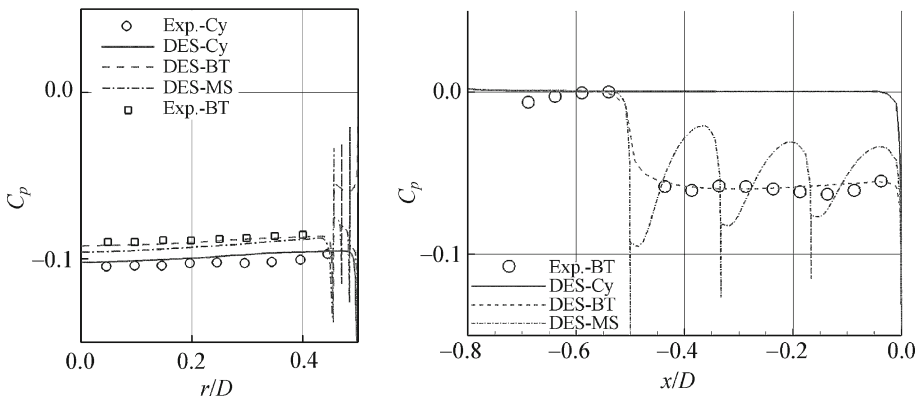

Fig. 7 The pressure on the base and the body around different aftbodies using DES

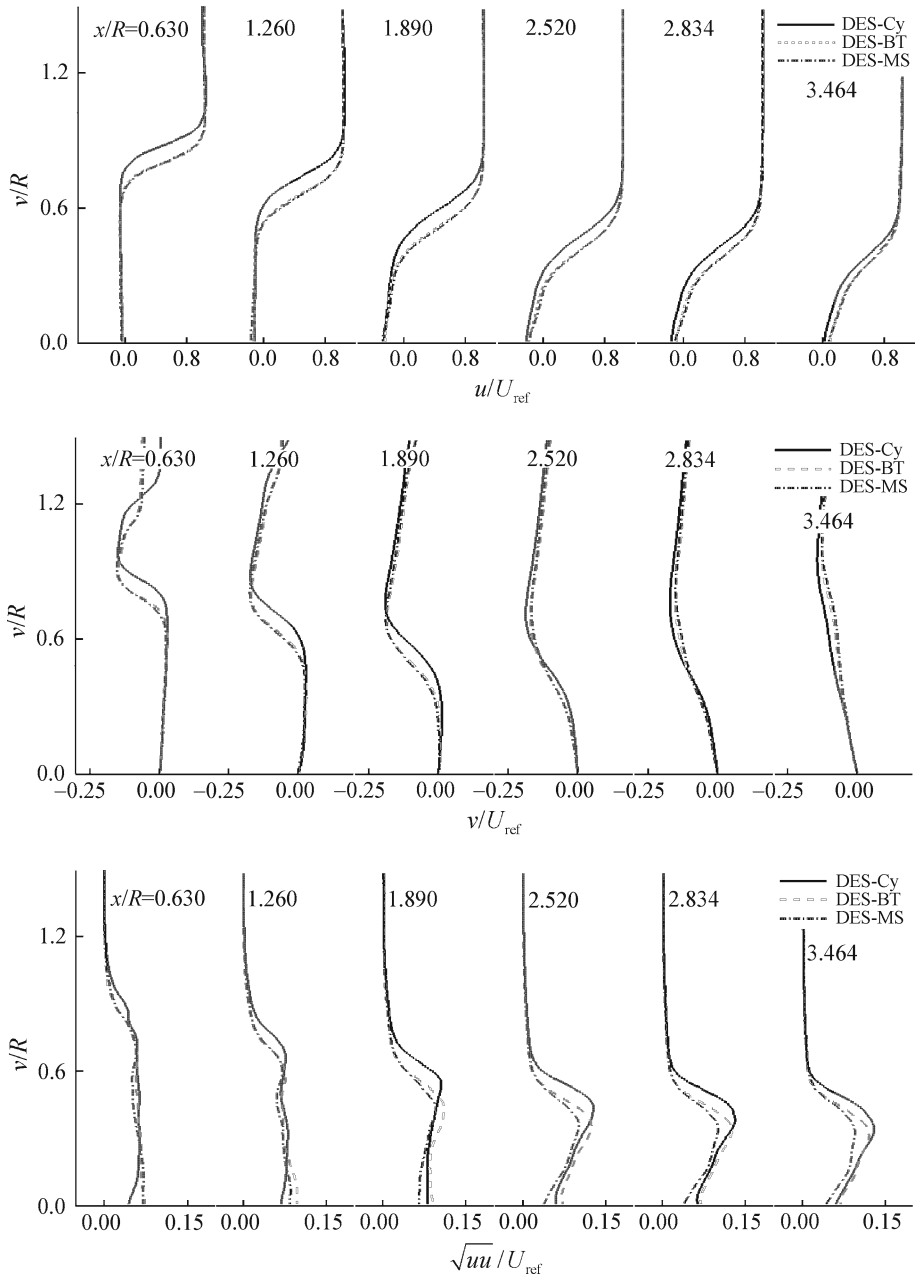

Fig. 8 The comparison on the streamwise and radial velocity and the streamwise normal stress

structures in the base wake are much weaker than those of BT and Cy.

End views of instantaneous Mach number distributions at the $x/R = 2.65$ and 4.5 downstream from the base computed by DES (Fig. 10, right) and a planar flow visualization image obtained experimentally by Bourdon and Dutton [7] using a Mie scattering imaging technique are shown in Fig. 10. As for the experimental planar visualization, because condensed ethanol droplets are suspended in the freestream, the high signal shows freestream and the low signal shows recirculation and a wake core region. Therefore, the border of the experimental image in Fig. 10 shows the end view shape of the instantaneous free shear layer. The computed turbulent structure caused by the instability of the shear layer shows the formation of mushroom-shaped patterns in the free shear layer. A similar structure is also observed in the experiment of Bourdon and Dutton. These results show the capability of the LES/RANS hybrid methodology for the prediction of unsteady flow features in contrast to unsteady RANS.

5 Conclusion

Flows around Cy, BT and MS afterbodies are investigated in this work with RANS and two RANS/LES hybrid (DES and DDES) methods based on SST model with compressible

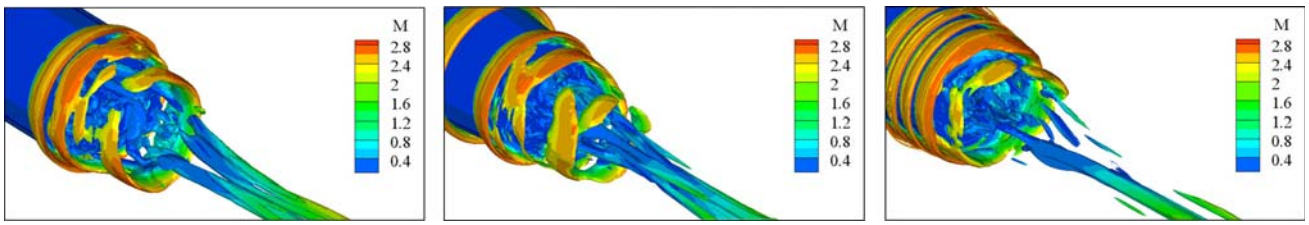

Fig. 9 The coherent structures behind the base around different afterbodies

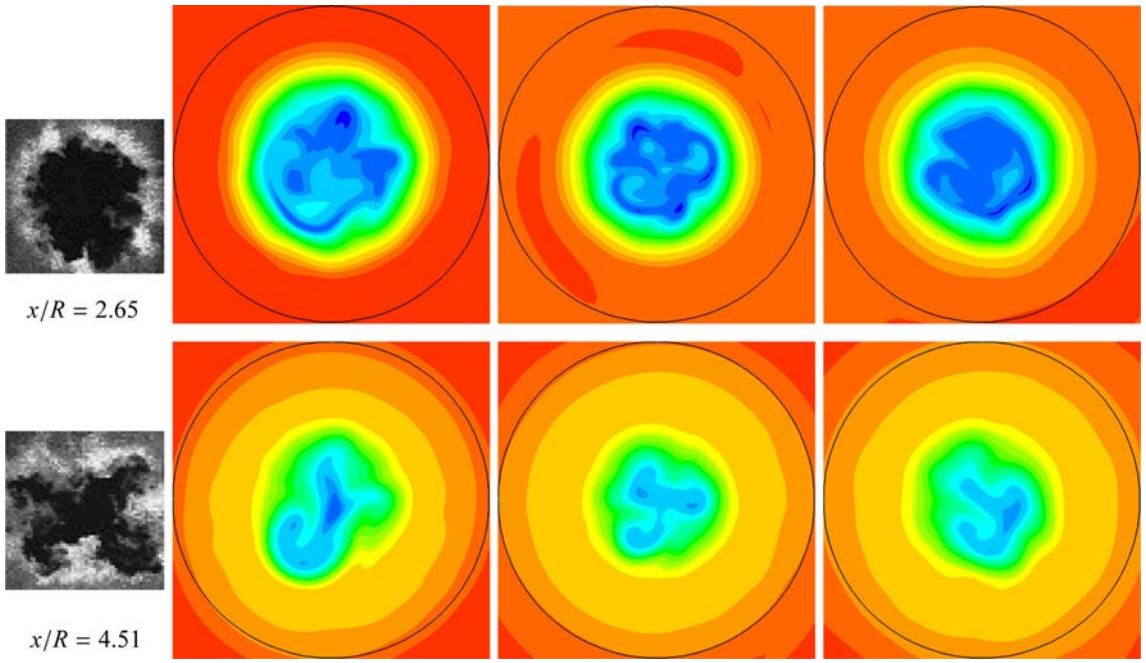

Fig. 10 Instantaneous end view images

modifications. While RANS can simulate the mean flow structure the RANS/LES hybrid methods can predict more satisfactorily the velocity, streamwise normal stress, and base pressure distribution. Instantaneous and chaotic structures can also be reasonably well captured by the RANS/LES hybrid methods, especially the thin helical structures in the shear layer behind the base. At the streamwise sections behind the base, the mushroom-like shear-layer structures are predicted which is present in the experiments.

Distinct pressure recovery can be achieved after using both BT and MS concepts. It means that considerable drag reduction can be obtained.

References

1. Mathur, T., Dutton, J.C.: Velocity and turbulence measurements in supersonic base flow with mass bleed. AIAA J. **34**, 1153–1159 (1996)
2. Hemin, J.L., Dutton, J.C.: Supersonic near-wake afterbody boattailing effects on axisymmetric bodies. J. Spacecr. Rockets **31**, 1021–1028 (1994)
3. Ruffin, S.M., Gupta, A., Marshall, D.: Supersonic channel airfoils for reduced drag. AIAA J. **38**, 480–486 (2000)
4. Viswanath, P.R.: Drag reduction of afterbodies by controlled separated flows. AIAA J. **39**, 73–78 (2001)
5. Mathur, N.B., Viswanath, P.R.: Drag reduction from square-base afterbodies at high speeds. J. Aircr. **41**, 811–820 (2004)
6. Herrin, J.L., Dutton, J.C.: Supersonic base flow experiments in the near wake of a cylindrical afterbody. AIAA J. **32**, 77–83 (1994)
7. Bourdon, C.J., Dutton, J.C.: Planar visualizations of large-scale turbulent structures in axisymmetric supersonic separated flows. Phys. Fluids **11**, 201–213 (1999)
8. Zhang, H.X., Li, Z.W.: Numerical simulation of hypersonic laminar wake. Acta Mech. Sin. **24**, 389-399 (1992) (in Chinese)
9. Suzen, Y.B., Hoffmann, K.A.: Investigation of supersonic jet exhaust flow by one- and two-equation turbulence models. AIAA Paper 98–0322 (1998)
10. Silton, S.I.: Navier–Stokes computation for a spinning projectile from subsonic to supersonic. AIAA paper 2003–3936 (2003)
11. Fureby, C., Nilsson, Y., Andersson K.: Large eddy simulation of supersonic base flow. AIAA paper 99–0426 (1999)
12. Sandberg, R.D., Fasel, H.: Direct numerical simulation of transitional supersonic base flows. AIAA paper 2005–0098 (2005)
13. Forsythe, J.R., Hoffmann, K.A., Cummings, R.M., Squires, K.D.: Detached-eddy simulation with compressibility corrections applied to a supersonic axisymmetric base flow. J. Fluids Eng. **124**, 991–923 (2002)

14. Kawai, S., Fujii, K.: Computational study of supersonic base flow using hybrid turbulence methodology. AIAA J. **43**, 1265–1275 (2005)
15. Xue, B.M., Yang, Y.: Technical details in applying DES method to computing supersonic cylinder-base flow. J. Northwestern Polytech. Univ. **24**, 544–547 (2006) (in Chinese)
16. Xiao, Z.X., Fu, S.: Study of the supersonic base flow using RANS/LES methods. Comput. Phys. (in press) (in Chinese)
17. Sparlart, P.R., Deck, S., Shur, M.L., Squires, K.D., Strelets, M., Travin, A.: A new version of detached-eddy simulation, resistant to ambiguous grid densities. Ther. Comput. Fluid Dyn. **20**, 181–195 (2006)
18. Strelets, M.: Detached eddy simulation of massively separated flows. AIAA paper 2001–0879 (2001)
19. Wilcox, D.C: Reassessment of the scale-determining equation for advanced turbulence models. AIAA J. **26**, 1299–1310 (1988)
20. Menter, F.R.: Two equation eddy viscosity turbulence models for engineering applications. AIAA J. **32**, 1598–1605 (1994)
21. Xiao, Z.X., Zhang, Y.F., Huang, J.B., Chen, H.X., Fu, S.: Prediction of separation flows around a 6:1 prolate spheroid using RANS/LES hybrid approaches. Acta Mech. Sin. **23**, 369–382 (2007)
22. Menter, FR, Kuntz, M: A zonal SST-DES formulation. DES-WORKSHOP (2003)
23. Xiao, Z.X., Chen, H.X., Zhang, Y.F., Huang, J.B., Fu, S.: Study of delayed-detached eddy simulation with weakly nonlinear turbulence model. J. Aircr. **43**, 1377–1385 (2006)
24. Fu, S., Xiao, Z.X., Chen, H.X., Zhang, Y.F., Huang, J.B.: Simulation of wing-body junction flows with hybrid RANS/LES methods. Int. J. Heat Fluid Flow **28**, 1379–1390 (2007)